

Two-Dimensional ^1H and ^{31}P NMR Spectra and Restrained Molecular Dynamics Structure of a Covalent CPI-CDPI₂-Oligodeoxyribonucleotide Decamer Complex[†]

Robert Powers and David G. Gorenstein*

Department of Chemistry, Purdue University, West Lafayette, Indiana 47907

Received May 2, 1990; Revised Manuscript Received July 18, 1990

ABSTRACT: CPI-CDPI₂ is a synthetic analogue of CC-1065, which is a naturally occurring antitumor antibiotic. Assignment of the ^1H NMR spectra of a CPI-CDPI₂-oligodeoxyribonucleotide decamer, d-(CGCTTAAGCG)₂, complex has been made by two-dimensional $^1\text{H}/^1\text{H}$ spectroscopy. The solution structure of the complex was calculated by an iterative hybrid relaxation matrix method combined with NOESY distance restrained molecular dynamics. Refinement proceeded in two steps in which the decamer was initially refined alone and then CPI-CDPI₂ was added to the structure to allow initial estimates of drug-DNA contacts. A hybrid matrix/MD refinement was used to better take into account problems associated with spin diffusion. Thus the distances from the 2D NOESY spectra were calculated from the relaxation rate matrix which were evaluated from a hybrid NOESY volume matrix comprising elements from the experimental spectrum and those calculated from an initial structure. The hybrid matrix derived distances were then used in a restrained molecular dynamics procedure to obtain a new structure that better approximates the NOESY spectra. The resulting partially refined structure was then used to calculate an improved theoretical NOESY volume matrix which is once again merged with the experimental matrix until refinement is complete. The efficacy of CC-1065 has been attributed to its minor groove binding and alkylation to the N3 position of adenosine. CPI-CDPI₂ appears to bind to the decamer in a similar manner. The effect of CPI-CDPI₂ on the decamer's ^1H and ^{31}P spectrum was consistent with a minor groove binding motif with the drug alkylating at A17 with the CDPI rings oriented toward the 5'-end of the alkylated strand. In addition, the NMR data support one major adduct but also indicate the presence of a minor adduct. The latter could represent a drug alkylation of the DNA at a secondary site (or alternative orientation of the rings).

CC-1065 is a naturally occurring antitumor antibiotic derived from *Streptomyces zelensius* (Hanka et al., 1978; Martin et al., 1980). The CC-1065 molecule (Figure 1) has a pseudotrimer structure with the central and right-hand segment corresponding to a PDE-I dimer (1,2-dihydro-3H-pyrrolo-[3,2-e]indole) and the left-hand segment corresponding to 4,4-spirocyclopropylcyclohexa-2,5-dienone (spirobicyclo-[5.2.0]octa-2,5-dien-4-one). The left-hand segment has a reactive cyclopropyl function. CC-1065 has shown exceptional potency in in vitro cytotoxic and antimicrobial activity and an in vivo antitumor activity (Adams et al., 1988; Moy et al., 1989; Wierenga et al., 1986). CC-1065 at 0.05 ng/mL causes 90% inhibition of L1210 cell growth compared to 4 ng/mL actinomycin D and 20 ng/mL adriamycin. CC-1065 causes an ~50% decrease in the colony-forming units of tumor cells from patients with cancer of lung, breast, pancreas, ovary, etc., at a concentration of 0.1 ng/mL. It is also 100-fold more lethal to B16 and CHO1 cells than adriamycin, actinomycin D, and *cis*-diamminedichloroplatinum. The use of CC-1065 as a therapeutic drug was ruled out when it was observed that CC-1065 exhibited a delayed hepatotoxicity which was fatal in mice. Current studies have dealt with understanding the factors that contribute to CC-1065 cytotoxicity and hepatotoxicity in an attempt to synthesize a CC-1065 analogue that would remove the delayed hepatotoxicity.

The activity of CC-1065 has been attributed to an interaction with DNA at the cellular level. The CD difference

spectra, NMR spectra, and UV melting profile results of CC-1065 binding to various macromolecules indicate that CC-1065 binds only to double-stranded B-DNA (Krueger et al., 1986, 1985; Krueger & Prairie, 1987; Swenson et al., 1982a) with a preference for AT base pairs, but it also binds strongly to a DNA triple helix (Krueger et al., 1985). The binding of CC-1065 to triple helix does not result in a strand separation to a B-DNA duplex and a single strand, suggesting that the drug binds in the minor groove of the triple helix. Further support for the minor groove binding of CC-1065 to B-DNA (Hurley & Needham-VanDevanter, 1986; Reynolds et al., 1986; Swenson et al., 1982b) was shown by the ability of netropsin, a known minor groove binding drug with a specificity for AT base pairs, to inhibit the binding of CC-1065 to B-DNA. Similarly, T4 phage DNA, which has 65% glycosylated cytosine residues in the major groove, binds CC-1065 as measured by the induced CD (Reynolds et al., 1986). CC-1065 also inhibits the alkylation of DNA by methyl-nitrosourea and ethylnitrosourea. Both methyl-nitrosourea and ethylnitrosourea alkylate the N3 of guanosine, the N3 of adenosine, and the O2 of cytosine in the minor groove of DNA.

Thus, CC-1065 is believed to initially bind reversibly in the minor groove. This is followed by irreversible alkylation between the N3 of adenosine and the cyclopropyl group of the left-hand segment (Reynolds et al., 1986; Hurley et al., 1990), concomitant with ring opening of the cyclopropyl group. After alkylation of the DNA it has been shown that the CC-1065 induces single-strand breaks at elevated temperatures.

The CC-1065 chromophore-DNA base-pair adduct has been isolated by heating the CC-1065-DNA complex at 100 °C for 30 min, followed by extraction with butanol (Krueger & Prairie, 1987; Reynolds et al., 1986). The ^1H and ^{13}C NMR spectra of the adenosine-CC-1065 adduct identified the point of attachment as the N3 of adenosine to the cyclopropyl

[†]Supported by NIH (AI27744), the Purdue University Biochemical Magnetic Resonance Laboratory which is supported by NIH (Grant RR01077 from the Biotechnology Resources Program of the Division of Research Resources), the NSF National Biological Facilities Center on Biomolecular NMR, Structure and Design at Purdue (Grants BBS 8614177 and 8714258 from the Division of Biological Instrumentation), and the National AIDS Research Center at Purdue (AI72713).

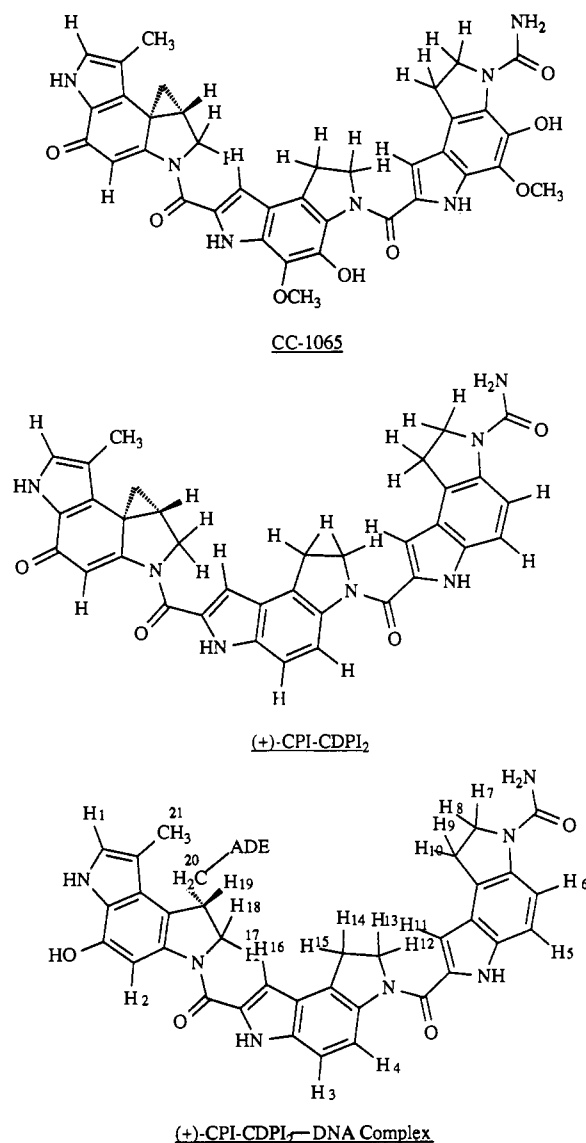


FIGURE 1: Structure of CC-1065 (top), (+)-CPI-CDPI₂ (middle), and the DNA-alkylated, ring-opened (+)-CPI-CDPI₂-duplex complex (bottom; numbering convention for the drug protons is shown).

methylene carbon of CC-1065. The nature of the strand cleavage was determined to be a single thermally induced β -elimination which occurs on the 3' side of the adenine to which CC-1065 was covalently bound. The heat-induced cleavage of DNA by CC-1065 (Hurley et al., 1987; Needham-VanDevanter et al., 1984; Reynolds et al., 1985) was used to determine the sequence selectivity of the drug by using the promoter element of SV40 DNA. The resulting consensus sequences were 5'-d(A/GNTTA)-3' and 5'-d(AAAAA)-3'.

The structure of CC-1065 has been determined by X-ray crystallography and ¹³C and ¹H NMR (Chidester et al., 1981). Although no X-ray structure of a complex is available,¹ CC-1065 may readily fit edge on into the minor groove and follow the natural curvature of the DNA. CC-1065 is well suited for this binding motif since the hydrophobic groups align the inside drug edge interacting with the hydrophobic minor groove pocket. The hydrophilic substituents are on the outside edge and interact with the polar solvent. Molecular modeling

of a CC-1065-DNA complex indicated that there is a snug fit of the drug in the minor groove and that the stereochemistry of the DNA–drug bond must be 3*bR*,4*aS* to accommodate the N3 adduct (Reynolds et al., 1986).

A series of CC-1065 analogues have been synthesized at Upjohn to analyze the components of CC-1065–DNA binding (Adams et al., 1988; Reynolds et al., 1986; Warpehoski et al., 1988). The analogues lacking the alkylating capability were relatively inactive. The truncated analogues, which were only dimers or monomers, had a slower rate of complex formation. An analogue with only the left-hand alkylating segment showed low cytotoxic effects. These results with the CC-1065 analogues clearly indicated an important role for both the cyclopropyl-containing moiety and the PDE-I dimer. A related series of CC-1065 analogues, such as (+)-CPI-CDPI₂ (Figure 1), have been synthesized and studied by Boger and co-workers (Boger & Coleman, 1988). These analogues have similar properties to those of CC-1065.

The factors that determine the anticancer activity, cytotoxicity, and the delayed hepatotoxicity of CC-1065 and related analogues are still unknown. The orientation of these drugs in the minor groove and the relative stereochemistry is largely unknown. The importance and role of alkylation and minor groove binding to the drug's efficacy have yet to be fully confirmed. In this paper a preliminary model of the CC-1065 analogue (+)-CPI-CDPI₂ bound to the decamer d-(CGCTTAAGCG)₂ has been determined by 2D NMR and NOESY distance restrained molecular dynamics. The decamer sequence was chosen on the basis of the footprinting studies of CPI-CDPI₂ with SV40 DNA (Boger et al., private communication).

EXPERIMENTAL PROCEDURES

Materials. The CC-1065 analogue (+)-CPI-CDPI₂ was provided by Dr. Dale Boger from the Chemistry Department at Purdue University (Boger & Coleman, 1988).

DNA Synthesis. The decamer d(CGCTTAAGCG)₂ was synthesized on a 10- μ mol scale and purified as previously described (Gait, 1984; Schroeder et al., 1987).

Small-Scale Preparation of the Decamer–CPI-CDPI₂ Complex. A CPI-CDPI₂–decamer sample for the UV and HPLC was initially prepared on the 1-OD (in 1 mL of buffer) scale. The buffer consisted of 10 mM phosphate, pH 7.0, 10 mM KCl, and 10% DMSO. The complex was prepared by incubating 2 μ L of a stock decamer solution (0.6 mg in 120 μ L of buffer) with 18 μ L of a stock drug solution (1.03 mg of CPI-CDPI₂ in 100 μ L of DMSO) at 37 °C for 5 days.

Large-Scale Preparation of the Decamer–CPI-CDPI₂ Complex for NMR. Larger amounts of the decamer–CPI-CDPI₂ for NMR were prepared by incubating ca. 5 μ mol of the decamer sample with 1.05 mol equiv of the CPI-CDPI₂ in 2.5 mL of buffer for 5 days at 37 °C. CPI-CDPI₂/DMSO mixture (250 μ L) was added to 2.25 mL of the DNA/buffer solution. Essentially, the same binding procedure was used as with the small-scale reaction. After 5 days, the reaction proceeded to only 50% completion. The extent of the reaction was monitored by HPLC and UV/vis spectroscopy. The mole equivalent of CPI-CDPI₂ was increased to 1.5 by adding 100 μ L of the CPI-CDPI₂/DMSO mixture, and the total volume was increased to 3.5 mL by adding 900 μ L of buffer. The reaction mixture was incubated for an additional 5 days at 37 °C. The reaction proceeded to 100% completion, as determined by HPLC and UV/vis spectroscopy, and demonstrates a 1:1 mole ratio for the complex.

UV Study of the Decamer–CPI-CDPI₂ Complex. The extent of bound CPI-CDPI₂ was measured by UV spectroscopy

¹ After completion of this study some preliminary 2D NMR work on a CC-1065 oligonucleotide duplex has been reported that is consistent with the minor groove binding and alkylation at N-3 of an adenosine (Scahill et al., 1990).

on a Cary 210 spectrophotometer. The CPI-CDPI₂ drug was insoluble in aqueous solutions and was only soluble in DMSO and DMF. The extinction coefficient of CPI-CDPI₂ was measured by dissolving a known amount of CPI-CDPI₂ in DMF and calculated from the OD at its maximum of 355 nm. The extinction coefficient of CPI-CDPI₂ was determined to be 34 000 M⁻¹ cm⁻¹. The extinction coefficient of the decamer was estimated to be 20 OD units/mg at 260 nm. A qualitative measurement of the extent of the decamer-CPI-CDPI₂ reaction was then monitored by the relative intensity of the absorbance at 260 and 355 nm.

HPLC Study of the Decamer-CPI-CDPI₂ Complex. The nature of the complex was also monitored by reverse-phase HPLC on a Spectra Physics HPLC. An Altech analytical reverse-phase C-18 column of length 25 cm, outer diameter of 1/4 in., and a particle size of 10 μm was used. An acetonitrile/TEAA buffer gradient of 1% acetonitrile/min from an initial 5% acetonitrile was used. The observed peaks were integrated with a Hewlett-Packard 3380A integrator and detected at 260 nm with an ISCO UV detector.

NMR Experiments. The ³¹P NMR spectra were acquired on a Varian XL-200 200-MHz spectrometer. The proton one-dimensional spectra, the two-dimensional States NOESY spectra (States et al., 1982), and the two-dimensional double-quantum-filtered COSY (DQF-COSY) (Piantini et al., 1982) were acquired on a Varian VXR-500 500-MHz spectrometer.

NMR Sample Preparation. The two NMR samples consisted of approximately 5 μmol of a decamer sample and a decamer-CPI-CDPI₂ (1:1) complex. The NMR samples were dissolved in 100 mM phosphate buffer, pH 7.0, 100 mM KCl, 1 mM EDTA, and 1 mM sodium azide in a total volume of 600 μL of 99.996% D₂O. The proton spectra were referenced to H₂O at 4.8 ppm. The ³¹P spectra were referenced to trimethyl phosphate at 0.00 ppm.

1D NMR Spectra of the Decamer and the Decamer-Drug Complex. The ¹H one-dimensional spectra of the decamer-drug complex was obtained with a sweep width of 6000 Hz and 24 000 data points. A 90° pulse width of 23.0 μs and a total recycle time of 4 s were used. The data were processed with 32K zero filling and a combination skewed sine bell-Gaussian apodization function to generate resolution enhancement.

The ³¹P one-dimensional spectra of the decamer and the decamer-drug complex were obtained with a sweep width of 800 Hz and 1600 data points. A 90° pulse width of 7.8 μs and a total recycle time of 2 s were used. The data were processed with 8K zero filling and a Gaussian apodization function to generate resolution enhancement.

The longitudinal relaxation times (*T*₁) of the decamer were measured from the inversion-recovery spectra (Canet et al., 1975). The spectra were acquired with a sweep width of 6000 Hz and a total recycle time of 42.5 s. A 90° pulse width of 24 μs and a corresponding 180° pulse of 48 μs was used. The data were collected with 30 016 data points and processed with 32K zero filling and 1 Hz of line broadening. The inversion-recovery spectra of the decamer-CPI-CDPI₂ complex were collected with a sweep width of 5000 Hz with 32K data points. A 90° pulse width of 20.5 μs and a corresponding 180° pulse width of 41 μs were used to acquire the spectrum. A recycle delay of 20 s was used which is adequate to measure a maximal *T*₁ of 5 s. The data were processed with 0.50 Hz of line broadening and zero-filled to 64K. The Varian VNMR software was used to fit exponential curves to the experimental data to evaluate *T*₁ times for the aromatic, H1'/H5, H4'/

H5'/H5'', H2'/H2'', and the methyl regions of the spectra.

Spectra of the exchangeable imino protons of the decamer and the decamer-CPI-CDPI₂ complex were measured by using the WS1D water suppression scheme (Sklenar & Bax, 1987). The sample was redissolved in 10% D₂O/90% H₂O, and the spectra were recorded over the temperature range of 5–35 °C. Spectra of the decamer-CPI-CDPI₂ complex were not taken over 35 °C because at higher temperatures the drug induces cleavage of the duplex. The spectra were collected with a 90° pulse length of 18.0 μs, a sweep width of 12 000 Hz, and 24 000 data points. The delay time between the 90° pulses was 0.000 15 s with a homospoil pulse of 0.006 s, and a recovery delay of 0.005 s was used to saturate the HDO signal and to selectively observe the imino resonances. A recycle delay of 1 s was used. The data were processed with 3 Hz of line broadening and zero-filled to 2K.

2D NMR Spectra of the Decamer-CPI-CDPI₂ Complex. The two-dimensional States NOESY spectra (States et al., 1982) of the decamer-drug complex were acquired at mixing times of 150, 250, and 400 ms. The 400-ms mixing time NOESY spectrum was collected for the assignment of the proton signals. The 250-ms NOESY spectrum was acquired to measure the volumes of the proton-proton NOE cross-peaks for distance determination. The 400-ms NOESY was acquired with a sweep width of 4498.1 Hz in both the *t*₁ and *t*₂ dimensions. The spectrum was collected as 512 FIDs (*t*₁) by 1984 data points (*t*₂). A 90° pulse width of 14.5 μs and a relaxation delay of 2.5 s were used. Sixteen transients were collected for each of the 512 FIDs. The spectrum was zero-filled to 2K in the *t*₂ dimension and zero-filled to 1K in the *t*₁ dimension. A Gaussian apodization function was applied in both the *t*₁ and *t*₂ dimensions to generate resolution enhancement. The data were collected with the sample non-spinning to avoid *t*₁ noise. The HDO solvent signal was saturated with the decoupler followed by a homospoil pulse during the *t*₁ period of the pulse sequence. The 250-ms States NOESY spectrum was acquired with a sweep width of 5998.8 Hz in both the *t*₁ and *t*₂ dimensions. The spectrum was collected as 256 FIDs by 2K data points. A 90° pulse width of 23.5 μs and a relaxation delay of 4.5 s were used. Eighty transients were collected for each of the 256 FIDs. The data were processed with 2K zero filling in both the *t*₁ and *t*₂ dimensions. A skewed sine bell apodization function was used in both the *t*₁ and *t*₂ dimensions, but no resolution enhancement was used. The apodization function was designed to simply eliminate FID truncation errors without decreasing the intensity of the first data point. A polynomial base-line correction was applied in both the *t*₁ and *t*₂ dimensions.

The DQF-COSY spectrum was acquired to assign the H5-H6 cytosine protons through their COSY coupling cross-peaks (Piantini et al., 1982). The DQF-COSY spectrum was measured with a sweep width of 4672.5 Hz in both the *t*₁ and *t*₂ dimensions. The spectra were collected as 1024 FIDs by 4032 data points. Eight transients were collected for each of the 1024 FIDs. A 90° pulse width of 12 μs and a relaxation delay of 2 s were used. The spectrum was collected with the sample non-spinning. The spectrum was processed with zero filling of 4K in the *t*₁ dimension and 2K in the *t*₂ dimension. A skewed sine bell apodization function was applied in both the *t*₁ and *t*₂ dimensions to generate resolution enhancement.

NOESY Distance Restrained Molecular Mechanics/Dynamics Calculations of the Drug-Duplex Complex. The initial Cartesian coordinates of the decamer were generated by using the NUCGEN module of AMBER3 (Weiner & Kollman, 1981) using Arnott right-handed B-DNA coordinates. The

program MIDAS (Ferrin & Langridge, 1980) operating on a Silicon Graphics Iris 3030 workstation was used for molecular modeling of the decamer and the complex. The standard AMBER3 force-field parameters were used for the decamer. The force-field parameters and structure for CPI-CDPI₂ was provided by Dr. Dale Boger to incorporate into the AMBER3 database. The CPI-CDPI₂ structure was initially modeled and energy minimized by use of MacroModel V2.5.

The CPI-CDPI₂ structure was docked to the decamer by using MIDAS. The CPI-CDPI₂ structure was positioned edge on, with its convex edge facing the minor groove. The drug was positioned in the minor groove with its curvature matching the DNA's curvature. The drug was positioned in such a way that the ring-opened cyclopropyl carbon was within 1.5 Å of the N3 nitrogen of A17. The docked structure was then minimized by using AMBER3.

NOESY distance constraints were incorporated into the potential energy force field through addition of a flatwell potential (Gorenstein et al., 1989; Powers et al., 1989). Only DNA distance constraints were used. The different model built structures with 149 DNA NOESY distance constraints from the 250-ms NOESY spectrum were then energy refined until a RMS gradient of 0.1 kcal/(mol·Å) was achieved or until the change in energy was less than 1.0×10^{-7} kcal/mol for successive steps. The energy minimization used the flatwell distance-constraining potential with an initial force constant of 20 kcal/mol with a permitted distance error of $\pm 10\%$. After the fourth iteration of refinement, the NOESY distance constraining force constant was increased to a final value of 30 kcal/mol and the permitted error decreased to a final value of $\pm 5\%$. A residue based cutoff and a distance dependent dielectric function were used. The latter approximates a solution dielectric constant for a gas-phase minimization. An 8.5-Å distance cutoff was used for nonbonded pair interactions. The 1–4 van der Waals and the 1–4 electrostatic interactions had a scale factor of 2.0. A full conjugate gradient minimization was calculated with an initial step length of 5×10^{-4} and a maximum step length of 1.0. The shake routine was not used.

Refinement utilized separate 5-ps cycles of AMBER3 molecular dynamics using the modified potential function which included the NOESY distance restraining flatwell potential. A Maxwellian distribution was used to calculate the initial velocities at 10 K. The time step for the integration was set to 1 fs, and coordinates were stored every 50 steps. The cutoff distance for nonbonded pairs was set to 8.5 Å, and a distance-dependent dielectric was used. The calculation was done at a temperature of 298.5 K. The calculations used velocity scaling and constant temperature. The 1–4 van der Waals and 1–4 electrostatics were scaled by a factor of 2.0. The charges on the 3' and 5' protons were modified to prevent unwanted bond formation. Again, the shake routine was not invoked. All energy minimization, hybrid matrix, and restrained molecular dynamics calculations were carried out on MicroVax II and III and Silicon Graphics Personal Iris computers.

Hybrid Matrix/MORASS Refinement of Structures. A relaxation matrix program (MORASS: Multiple Overhauser Relaxation Analysis and Simulation) (Post et al., 1990; Meadows et al., 1989; Gorenstein et al., 1990; Nikonowicz et al., 1989; the program is available upon request) was used to calculate volume and rate matrices as well as implement the hybrid matrix methodology. The later method (Boelens et al., 1988, 1989; Gorenstein et al., 1990; Nikonowicz et al., 1989) allows for iterative refinement of the structure until there is no further convergence between the experimental and theo-

retical NOESY spectra. In this method the well-resolved and measurable cross-peaks in the NOESY spectrum replace the corresponding cross-peaks in the calculated volume matrix (theoretical NOESY spectrum), while overlapping or weak cross-peaks and diagonals are from the calculated spectrum. This hybrid volume matrix, V^{hyb} , is then used to evaluate the rate matrix, whose off-diagonal elements include the effects of spin diffusion. Distances derived from this hybrid relaxation rate matrix (we assume a single isotropic correlation time of 4.0 ns) are then utilized as distance constraints in a 5-ps restrained molecular dynamics simulation. Energy minimization of the averaged, last 3-ps structures derived from molecular dynamics completes one cycle of refinement. This process is repeated until a satisfactory agreement between the calculated and observed cross-peak volumes is obtained. As shown by our laboratory (Gorenstein et al., 1990; Nikonowicz et al., 1989) and Kaptein and co-workers (Boelens et al., 1988, 1989), 3–8 iterations appear to be adequate to achieve convergence to a "refined" structure.

Convergence is monitored by using eq 1 and 2. The latter criterion is analogous to that used in X-ray crystallography.

$$\%RMS_{vol} = \sqrt{\frac{1}{N} \sum_{ij} \left(\frac{v_{ij}^e - v_{ij}^{exp}}{v_{ij}^e} \right)^2} \times 100\% \quad (1)$$

$$R \text{ factor} = \frac{\sum_{ij} |v_{ij}^{exp} - v_{ij}^e|}{\sum_{ij} v_{ij}^{exp}} \quad (2)$$

Convergence is achieved when the $\%RMS_{vol}$ is within the reliability of the experimental volume measurement. $\%RMS_{vol}$ values were calculated with the theoretical volumes (v_{ij}^e) in the denominator of eq 1 [$\%RMS(TH)$] as well as the experimental volumes, v_{ij}^{exp} [$\%RMS(EXP)$]. Because most structurally important distances are those from longer range NOEs, and because these small off-diagonal volumes (<2% of the diagonal volumes) are the most sensitive to experimental noise, we feel an acceptable RMS error is 20–60% with an R factor of comparable size.

Initially, the hybrid matrix/MORASS refinement of the structure was applied to the intact CPI-CDPI₂–decamer complex. This resulted in a system which would not converge; in fact, it tended to diverge significantly, with the observed $\%RMS$ increasing from 100% to 300% over a short number of iterations. This was attributed to the large motion observed by the drug during the dynamics calculations. This motion resulted in the drug flipping from an edge-on complex to a face-on complex, which greatly distorted the DNA structure. "Freezing out" the motion of the drug during the dynamics runs eliminated the divergent nature of the refinement, but the system still did not converge. Convergence was only achieved when the drug was removed from the system. This was reasonable since only experimental DNA–DNA NOEs were used. The close proximity of some of the drug's protons to DNA protons in the initial model was probably distorting the MORASS restrained MD calculations. This resulted in a distorted DNA structure which could not fit the experimental NOE volumes and which provided a high kinetic barrier for the restrained MD simulations to locate the correct global minimum family of conformations. After the decamer structure converged, the CPI-CDPI₂ structure was redocked onto the decamer and refinement continued for a few more MORASS/MD cycles. The previously observed problems were eliminated. The tendency for the drug to flip in the minor groove from edge on to face on did not occur, and it was

possible to further define the structure by using the MO-RASS/hybrid matrix protocol.

RESULTS AND DISCUSSION

NMR Assignments of the Decamer-CPI-CDPI₂ Complex.

(A) DNA Assignments. The assignment of the proton spectrum of the decamer sequence d(CGCTTAAGCG)₂ and the decamer-CPI-CDPI₂ complex were made by the sequence-specific (Broido et al., 1984; Feigon et al., 1983; Frechet et al., 1983; Hare et al., 1983; Kearns, 1984; Scheek et al., 1984; Schroeder et al., 1986, 1987) methodology. An expansion of the 2D NOESY spectrum in the base to H1' region is shown in Figure 2, and additional spectra are provided in the supplementary material, Figures 1 and 2. The assignment of the proton and phosphorus spectra of the decamer sequence has been previously reported (Powers et al., 1990).

The ¹H assignment of the DNA component of the decamer-CPI-CDPI₂ complex also followed the sequence-specific protocol. The presence of the drug complicated the DNA assignments by eliminating the signal degeneracy between the two palindromic strands in the NMR spectrum. Thus, instead of 10 H8/H6 resonances in the decamer, 20 resonances were observed for the complex (compare panels A and B of Figure 2). Both DNA strands of the complex were assigned separately. The loss of degeneracy in the NOESY spectrum also indicates a successful binding of CPI-CDPI₂ to the decamer. The numbering convention for the decamer-CPI-CDPI₂ complex is shown, with the top strand identified as the A strand and the bottom the B (alkylated) strand:

5'-C1	G2	C3	T4	T5	A6	A7	G8	C9	G10-3'	A strand
3'-G20	C19	G18	A17	A16	T15	T14	C13	G12	C11-5'	B strand

The assignment of the decamer signals in the complex initially used the decamer's assignment as a template. This was particularly useful for the end bases where little changes in the chemical shifts were expected.

The cytosines were first identified by the five H5-H6 COSY cross-peaks in the DQF-COSY spectrum which corresponded to identical NOESY cross-peaks. The thymidines which are normally identified by the H6 to methyl cross-peaks in the NOESY spectrum could not be initially unambiguously assigned because of the upfield shifts incurred by the H2'/H2'' protons. This resulted in the methyl cross-peaks becoming part of the H8/H6 to H2'/H2'' region instead of being distinct. It was also not possible to immediately assign the adenosine H8 protons, which are generally the most downfield resonances, because the effect on the base's chemical shifts by the drug were unknown.

Because only the cytosine base resonances were assigned, a different approach was required to assist in the assignment of the NOESY spectrum. As observed in the NMR spectrum of the decamer, a guanosine to the 5' end of cytosine showed an NOE cross-peaks between the guanosine H8 proton and the cytosine H5 proton. This NOE pattern was seen extensively in the decamer-CPI-CDPI₂ NOESY spectrum and resulted in an important key to assigning the spectrum. This allowed for the assignment of 5'-G-C-3' pairs.

The decamer sequence d(CGCTTAAGCG)₂ contains three cytosines. Because of strand asymmetry in the CPI-CDPI₂ complex, there are six possible unique cytosine H6/H5 resonances. The DQF-COSY spectrum contained five distinct cytosine H6/H5 cross-peaks. The cross-peak corresponding to a cytosine H6 resonance at 7.51 ppm was more intense relative to the other H6/H5 cross-peaks. This was also seen in the NOESY spectrum, which indicated that this resonance corresponds to two degenerate cytosine H6/H5 protons. By

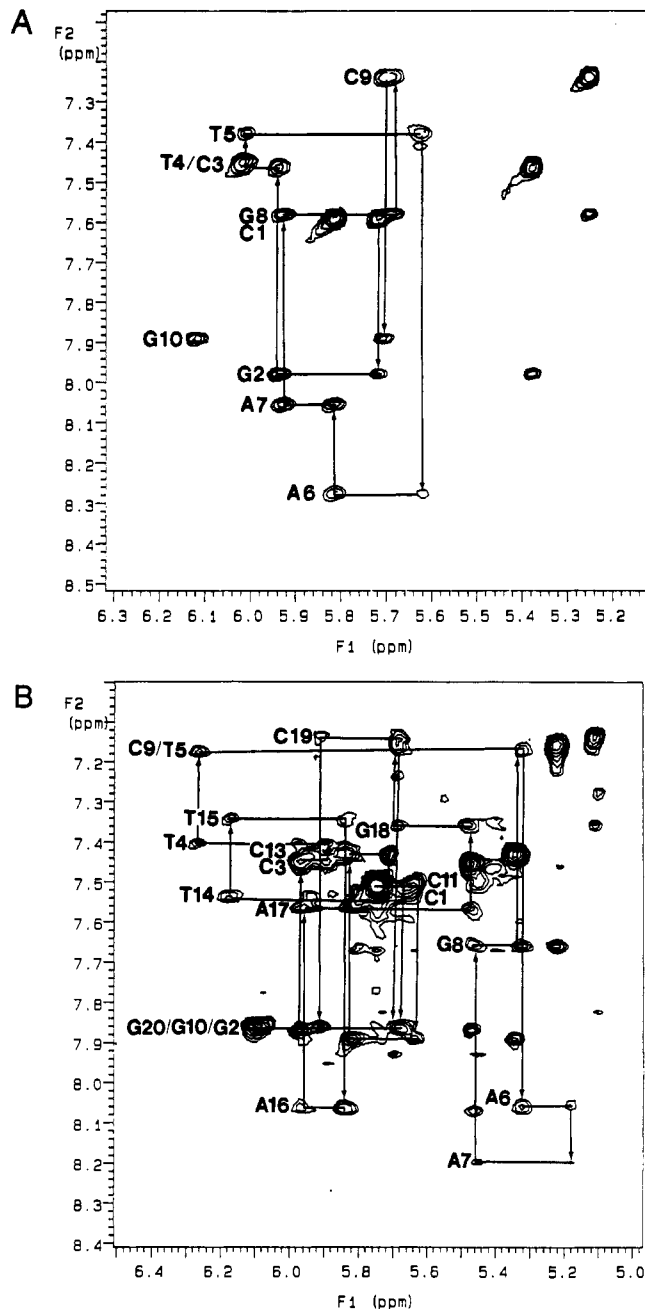


FIGURE 2: Pure absorption phase 400-ms ¹H/¹H NOESY NMR spectrum of duplex decamer-CPI-CDPI₂ at 500 MHz. (A) The base H8/H6 to H1' expanded region of the decamer alone. (B) The base H8/H6 to H1' expanded region of the decamer-CPI-CDPI₂ complex. The sequential connectivity of the base H8/H6 and deoxyribose H1' is diagrammed.

comparing the H8/H6 to H1' NOESY region of the decamer and the decamer-CPI-CDPI₂ spectra, the cytosine H6 resonance at 7.51 ppm was assigned to C1 and C11, which correspond to the 5' end cytosines of each strand. As previously described, the 5' end base should only contain one NOE to its own H1' proton, which was consistent with the observed number of NOEs for the H8/H6 resonance at 7.51 ppm. This further established the assignment of the resonance at 7.51 ppm to C1 and C11.

Because of the complexity of the decamer-CPI-CDPI₂ spectrum, each step of the sequential assignment was continuously verified from the H1'-H2'/H2'' region and the H8/H6-H2'/H2'' region. Thus, an inter H8/H6-H1' assignment was required to be internally consistent before the next assignment was made.

The sequential assignment of the DNA protons in the decamer–CPI–CDPI₂ complex began at C1 and C11. The intra H6–H1' (5.66/5.64) NOE of C1 and C11 showed a clear connectivity to two sets of NOEs, which were assigned to the guanosines. These H8/H6 (7.86/7.89) resonances were assigned to guanosines because of the presence of G H8 to C H5 (5.47/5.34) cross-peaks. The H8/H6–H1' NOE between C1/C11 and these guanosines and the G H8 to C H5 NOE of these guanosines to a pair of cytosines established the C1–G2–C3 and C11–G12–C13 connectivities. The assignment of G2/G12 to C3/C13 was further established by the inter H6 (7.45/7.43) to H1' (5.98/5.82) NOE from the C3/C13 H6 to the G2/G12 H1' protons. There were two possible connectivities from G2 to C3; the relatively downfield cross-peak was assigned to the connectivity between G2 and C3 because of the better alignment of these cross-peaks. The relatively upfield NOE (5.91) was better aligned, with a cross-peak to C19. This connectivity was required since the large NOE at 6.09 ppm was assigned to the intra H8 to H1' NOE of G10 and G20. This assignment was made by comparison of the decamer spectra to the decamer–CPI–CDPI₂ complex spectra. Since these resonances corresponded to terminal bases, only moderate changes in their chemical shifts were expected. In addition, the NOE volumes were very large relative to the other NOEs in this region, which was consistent with assigning this NOE to two degenerate resonances. Reversing this assignment also caused an inconsistency in the H2'/H2'' assignments in the H1'–H2'/H2'' and H8/H6–H2'/H2'' regions.

The sequential assignment continued with a connectivity to a thymidine in each strand. The H6 (7.45) to H1' (6.27) inter NOE between C3 and T4 showed a distinct connectivity. The assignment of the resonance at 7.41 ppm to a thymidine (T4) was further established by a cross-peak in the H8/H6–H2'/H2'' region which could be reasonably assigned to a H6 to methyl (1.58) NOE. The connectivity from C13 to T14 was not as clearly established as the C3 to T4 connectivity. The C13 H6 resonance showed a strong NOE to its own H1' (5.74) proton which should show a connectivity to T4's H6 proton. The NOE corresponding to an H1' of 5.74 ppm only showed a connectivity to the large, overlapping NOE region. Since C13 was making a connectivity to T14 and T14 makes a connectivity to T15, the next corresponding base assignment must show a reasonable H6 to methyl NOE. There were two possible paths out of this overlapping NOE region; only one path corresponded to the H6 to methyl NOE requirement. In addition, the relative chemical shift of T14's H6 proton corresponded to the chemical shift of T4 in the decamer spectra. Both T4 and T14 gave a clear and distinct connectivity to T5 and T15 via a H6 (7.17/7.34) to H1' (6.27/6.17) NOE. The thymidine connectivities were verified by the H6 to methyl NOEs (1.59, 1.64, 1.69) for T5, T14, and T15, respectively.

The connectivity continued from a thymidine to an adenosine in the sequential assignment. Both the T5 and T15 H6 to H1' (5.32/5.84) intra NOE showed connectivities to two possible NOE cross-peaks. For T15, one NOE had been previously assigned to the C3 H6 to its own H1'. Thus, the other connectivity to an H8/H6 resonance at 8.06 ppm was assigned to A16. For T5, one NOE corresponded to a guanosine as assigned by the G H8 to C H5 NOE connectivity. The remaining NOE cross-peak at 8.06 was assigned to A6. The fact that the H8 resonances of A6 and A16 were degenerate supported their assignments, since these resonances were degenerate in the decamer spectra because of symmetry. Even though the H8 resonances were degenerate, the effect

of the drug was seen in the H1' chemical shift dispersion (5.18/5.98) of 0.80 ppm. The assignment of A7 and A17 was determined by the inter H8 to H1' connectivity and by default, since the remaining resonances were assigned to a guanosine or a cytosine.

Both A6 and A16 showed clear connectivities to A7 and A17 through the H8 (8.29/7.56) to H1' (5.18/5.98) inter NOE. The chemical shift of the A7 H8 resonance was consistent with a typical adenosine H8 resonance, whereas the A17 H8 resonance had been significantly shifted upfield and probably corresponded to the adenosine to which CPI–CDPI₂ was covalently attached. It is interesting to note that, whereas adenosines 6 and 16 had degenerate H8 protons and the chemical shifts of the H1' protons were greatly perturbed by the drug, the converse was true for A7 and A17.

The connectivity continued to the second 5'-G-C-3' pair determined by the G H8 to C H5 NOE. The A7 and A17 H8 resonances were easily connected to G8 and G18 via the inter H8 (7.16/7.36) to H1' (5.47/5.97) NOE. Besides the G H8–C H5 NOE, the G8/G18 to C9/C19 connectivity was further established by the inter H6 (7.17/7.14) to H1' (5.32/5.69) NOE. The sequential assignment from G8 to C9 used the same NOE cross-peak as the assignment of T5 to A6. This overlapping path of assignments was confirmed by the presence of two sets of H1'–H2'/H2'' protons for the H1' proton of chemical shift 5.32 ppm. A similar overlap was seen with the G10 H8 to C9 H1' NOE and the C1 H1' to G2 H8 NOE. As with the other overlap, the connectivity was confirmed by the existence of two sets of H1'–H2'/H2'' peaks for the H1' proton of chemical shift 5.66 ppm. This completed the sequential assignments and further supported the degeneracy of the G10/G20 H8 resonance.

As previously stated, the H8/H6 to H1' sequence connectivity was verified with a consistency of the H2'/H2'' assignments in the H1'–H2'/H2'' and the H8/H6–H2'/H2'' region. The assignment of the H2'/H2'' resonances allowed for the identification of the inter H8/H6 to H2'/H2'' NOEs. The sequential assignments in the H8/H6 to H2'/H2'' region were used to verify and support the H8/H6–H1' assignments.

Additional information for the assignment of the decamer in the decamer–CPI–CDPI₂ complex was obtained from the base to base NOESY region (spectrum not shown). There were two prominent NOE cross-peaks in this region that corresponded to drug aromatic protons. This was verified by the presence of COSY cross-peaks in the DQF-COSY spectrum. These cross-peaks correspond to NOEs between protons with chemical shifts of 8.23 and 7.53 ppm, and 7.88 and 7.44 ppm. Base to base NOEs of DNA only occur between neighboring bases on the same strand. This region also contained sequential information which was consistent with the assignments in the H8/H6 to H1' region. NOES were seen between T4 and T5, and G8 and C9. There was a streak of NOEs that corresponded to connections between A16 and A17, A6 and A7, and T5 and A6. An NOE was also seen between G20 and C19. There was an additional NOE which could correspond to a connectivity both/either between C1 and G2 and/or between C19 and G20.

The remainder of the resonances were assigned as previously described. The H1' and H8/H6 resonance gave a connection to H3', H4', and H5'/H5''. The relative chemical shifts of H3', H4', and H5'/H5'' were still tentatively assigned in the order of H3' > H4' > H5'/H5''. Additional H3' and H4' resonances were determined from resolved H3'–H2'/H2'', H4'–H2'/H2'', and H3'–H4' NOEs. The assignment of the decamer proton signals also used a pure absorption phase

Table I: Nonexchangeable Proton Chemical Shifts^a (ppm) of the d(CGCTTAAGCC)₂-CPI-CDPI₂ Complex

base	H6/H8	H2	H5	H1'	H2'/H2''	H3'	H4'	H5'/H5''	CH3
C1	7.52		5.74	5.66	1.75/2.29	4.61			
G2	7.86			5.98	2.77/2.58	4.95	4.33		
C3	7.45		5.47	5.89	2.06/2.46	4.66	4.28	4.10/	
T4	7.41			6.27	2.25/2.45	4.25	4.09	3.99/	1.58
T5	7.17			5.32	1.85/1.91	4.34	4.04	3.79	1.59
A6	8.06			5.18	2.28/2.28	4.58	4.35		
A7	8.19	8.08		5.47	2.66/2.76	3.86	3.70	3.48/	
G8	7.66			5.32	2.16/2.46	4.61	4.08		
C9	7.17			5.69	1.84/2.29	4.62	4.04	3.79/	
G10	7.86			6.09	2.30/2.56	4.64	4.18		
C11	7.80			5.64	1.80/2.29	4.61	3.99		
G12	7.89			5.82	2.61/2.61	4.92	4.29		
C13	7.43			5.74	1.75/2.29				
T14	7.54			6.17	2.25/2.60	4.25	4.09	4.04/	1.64
T15	7.34			5.84	2.58/2.39				1.69
A16	8.06	7.40		5.98	2.43/2.68	4.58	4.35		
A17	7.56	7.24		5.47	2.13/2.46	4.48	3.58		
G18	7.36			5.69	2.20/2.29	4.48			
C19	7.14		5.12	5.91	1.82/2.34	4.61	4.28	4.10/	
G20	7.86			6.09	2.30/2.56	4.64	4.18		

^a Proton chemical shifts referenced to HDO at 4.80 ppm.

constant-time heteronuclear correlation (PAC) spectrum (Powers et al., submitted for publication) to assign H3' and H5'/H5'' protons. This was not possible with the decamer-CPI-CDPI₂ complex. The concentration of the same was too dilute to obtain a PAC spectrum. The nearly complete ¹H NMR assignments of the decamer in the decamer-CPI-CDPI₂ complex are listed in Table I.

(B) *CPI-CDPI₂ Assignments.* We experienced great difficulty in assigning the CPI-CDPI₂ resonances in the decamer-CPI-CDPI₂ complex because the CPI moiety and each of the two CDPI ring systems were essentially isolated spin systems with no information on their connectivity. In addition, we observed many more NOESY cross-peaks than could be explained by the DNA-DNA, drug-drug, and DNA-drug contacts if only one complex was present. Ultimately we came to realize that a number of these cross-peaks not previously assigned to the DNA represented cross-peaks from a minor adduct or conformational isomer (10–15%; see below). The aromatic *J*-coupled protons (H3, H4, H5, and H6; see Figure 1) could be unambiguously assigned as a set only and identified by the distinct COSY and NOESY cross-peaks along the diagonal in the aromatic region. None of these showed any NOESY or COSY connectivity to any other protons in the rest of the drug although some cross-peaks with DNA protons are observed.

The preliminary assignment of the other CPI-CDPI₂ resonances was based upon the CPI-CDPI₂ spin systems which predict a network of NOE cross-peak connectivities. The expected NOE connectivities between the drug resonances was initially based upon measured interproton distances from the CPI-CDPI₂ model structure. Any measured distance less than 3.5 Å would be expected to exhibit a relatively strong NOE cross-peak. The tentative assignment of the other CPI-CDPI₂ resonances were also based upon the assignment of the ¹H NMR spectrum of CPI-CDPI₂ in DMSO. Of course, the CPI-CDPI₂ resonances in the complex would be expected to be affected by the solvent change from DMSO to H₂O and from the binding of the drug to the duplex. In addition, the assignment of CPI-CDPI₂ resonances was assisted from expected drug to DNA NOESY cross-peaks determined from the final MORASS refined structure (see below). The sugar and adenosine H2 protons of the decamer were within 5 Å of CPI-CDPI₂ protons in the complex. A few NOE cross-peaks between the H1' protons of the duplex and the CPI-CDPI₂

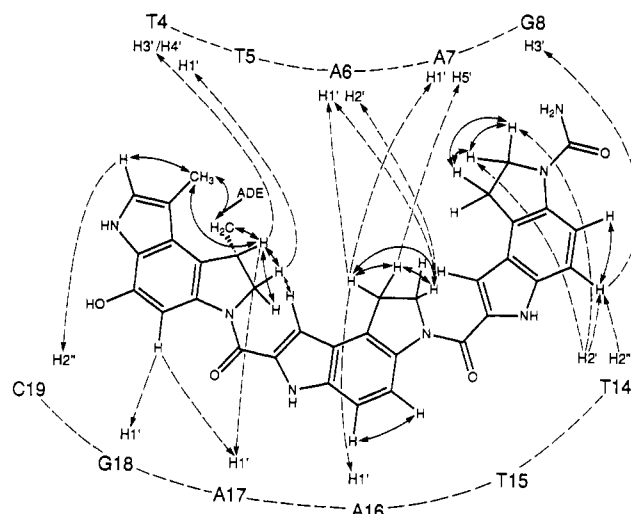


FIGURE 3: Structure of the decamer-CPI-CDPI₂ complex showing the cyclopropane ring opened N3-alkylated adenosine (17) and a partial listing of various drug-drug and drug-DNA contacts identified by NOESY cross-peaks (arrows).

protons were observed, which assisted in the assignment of some drug resonances. From the expected NOE cross-peak intensities based upon the final decamer drug model and the relative chemical shifts of CPI-CDPI₂, it was possible to make a set of preliminary assignments of some of the CPI-CDPI₂ resonances in the complex (Table II). Most of the observed set of tentative NOESY drug contacts are diagrammed in Figure 3.

On the basis of the contacts of the decamer to the assigned CPI-CDPI₂ resonances the drug clearly binds within the minor groove of the decamer, making contacts with C19 through T14 on strand B. Additional preliminary contacts are made from G8 to T4 on strand A. The CPI ring is in closest contact with A17, and in the model described below we assume that cyclopropyl ring opening has alkylated N3 of A17 with the CDPI rings oriented toward the 5' end of strand B of the duplex (Figure 3).

The drug-drug and DNA-drug NOESY cross-peak volumes relative to the strong (s) cytosine 3 H5/H6 cross-peak are also provided in Table II. The DNA-DNA proton distances calculated from the NOESY cross-peak volumes, by using a simple two-spin analysis of the NOESY spectrum and

Table II: Preliminary ¹H Chemical Shifts and NOESY Cross-Peaks of CPI-CDPI₂-Decamer Duplex Complex

CPI-CDPI ₂ proton	CPI- CDPI ₂ ^a	CPI-CDPI ₂ -decamer adduct ^b	drug cross-peaks ^c	DNA cross-peaks
H1	6.99	7.49	H21 (s)	C19 H2'' (m)
H2	6.79	7.93		G18 H1' (m), A17 H1' (w)
H3	8.39	8.22	H4 (s)	A6 H2' (m), A7 H5' (m)
H4	7.48	7.53	H3 (s)	
H5	8.14	7.88	H6 (s)	G8 H3' (s) ^d
H6	7.38	7.43	H5 (s)	T14 H2' (m) ^d
H7	4.15	3.84	H8 (s), H10 (s)	
H8	4.15	3.92	H7 (s), H9 (s), H10 (s)	T14 H2' (s), ^d T14 H2'' (m) ^d
H9	3.40	3.32	H8 (s), H10 (s)	
H10	3.40	3.50	H7 (s), H8 (s), H9 (s)	T14 H2' (s), ^d A6 H1' (w) ^d
H16	7.26	7.20	H17 (m), H18 (w)	
H17	4.57	4.33	H16 (m), H18 (s), H19 (s), H21 (s)	
H18	4.57	3.44	H16 (w), H17 (s), H19 (s)	T4 H1' (m)
H19	1.49	1.58	H17 (s), H18 (s), H21 (s), H20B (s)	A17 H1' (m), T4 H3' (w), T4 H4' (w)
H20A	2.04 ^e	3.84	H21 (m), H20B (s)	
H20B	3.24 ^e	4.66	H19 (s), H20A (s), H21 (s)	
H21	2.07	2.48	H1 (s), H19 (s), H20A (m), H20B (s)	

^a From Boger and Coleman (1988); in DMSO. ^b This work; in aqueous buffer. Data are insufficient to uniquely identify aromatic protons or geminal protons. ^c s, strong; m, medium; w, weak relative to C3 H5/H6 (s) cross-peak. ^d These contacts are mutually inconsistent with a single model and suggest that the second CDPI ring is conformationally mobile. ^e Cyclopropyl chemical shifts.

Table III: DNA–DNA Proton Distances (Å) Measured from NOESY Spectrum and Derived from a Two-Spin Analysis of the Spectrum

Intranucleotide Distances (R_{ij}) ^a							
base	H6/H8 to H1'	H6/H8 to H2'/H2''	H6/H8 to H3'	H1' to H2'/H2''	H1 to H3'	H3' to H2'/H2''	miscellaneous
C1		-/2.54		2.79/-		2.48/-	H6-H5 2.44
G2	4.09	2/87/2.35		2.76/2.53	3.27	2.38/2.30	H4'-H2'' 2.69
C3	3.26	2.79/2.72	3.47	2.87/2.56		2.66/-	
T4	3.70	2.46/2.55	3.98	2.81/2.63		2.88/-	
T5		-/2.96		2.90/2.87	3.86	2.81/3.05	
A6	4.21		3.59				
A7	4.29	2.60/2.55	3.98	3.12/3.03			H2-H1' 4.03
G8	3.47	2.65/2.86	3.57	2.79/2.55			
C9	4.03	-/2.93	3.17	2.82/-			H6-H5 2.45
G10							
C11		-/2.54		2.96/2.26	3.27		
G12	3.70		3.53		3.31		
C13	3.14	-/2.96		3.89/3.09			H6-H5 2.35
T14	3.51	2.53/2.62	3.72	2.74/2.57		2.39/2.77	
T15	3.69			2.61/2.39			
A16	3.90	2.44/2.57		2.51/2.49		-/2.79	H2-H1' 3.47
A17	3.49	2.66/2.67	3.70	3.10/2.69		2.62/2.85	
G18	4.23	2.47/2.61	3.53	2.82/-			
C19	3.27	2.44/2.77	3.13	2.93/2.42	3.86		H6-H5 2.65
G20							

Internucleotide Distances (R_{ij}) ^a							
base	H6/H8 to H1'	H6/H8 to H2'/H2''	miscellaneous	base	H6/H8 to H1'	H6/H8 to H2'/H2''	miscellaneous
C1				C11			
G2			H8-H5 4.03	G12	4.59	3.36/3.05	H8-H5 4.47
C3	3.06	3.00/2.78	H5-H2'' 2.63, H5-H1' 3.55	C13	2.90		H5-H1' 3.42
T4	3.01	2.58/-		T14		-/2.72	
T5	3.27	-/2.43		T15	3.44	-/2.83	
A6	3.53	3.11/3.03		A16	3.70	-/2.38	
A7	3.90			A17	3.59	2.67/2.78	H2-H1' 3.57
G8	3.55	3.11/3.63		G18	3.23	2.56/2.65	H8-H5 4.03
C9			H5-H2' 3.01, H5-H2'' 3.51	C19	3.33	2.50	H5-H2' 2.76, H5-H2'' 2.44, H5-H1' 3.70
G10				G20	3.55		

^a All distances referenced to C3 (H5/H6) cross-peak, assuming a reference distance of 2.45 Å.

by referencing to the known fixed distance of the cytosine 3 H5/H6 cross-peak, are also provided in Table III. The relative distances and cross-peak volumes are generally consistent with this preliminary model.

Even after most of the DNA–DNA, drug–drug, and DNA–drug cross-peaks are identified, a number of additional, unidentified NOESY cross-peaks remain throughout the spectrum. The majority of these peaks are weak and have chemical shifts similar to those of the drug–duplex complex. Indeed, in a number of instances fragments of expected base to sugar sequential connectivity and drug–drug connectivity

pathways are observed. None of the unidentified resonances have chemical shifts identical with those of the free decamer, ruling out a small impurity of unmodified decamer in the sample (confirmed by HPLC). Note even the cytosine H5/H6 cross-peaks in Figure 2B show overlap with some low-intensity unidentified shoulders to the cross-peaks. Thus the NMR data support one major adduct (80–85%), but also indicate the presence of a minor adduct. The latter could represent a drug alkylation of the DNA at a secondary site or alternative orientation of the drug in the minor groove. Because the spectra of the original sample remain unchanged over a period

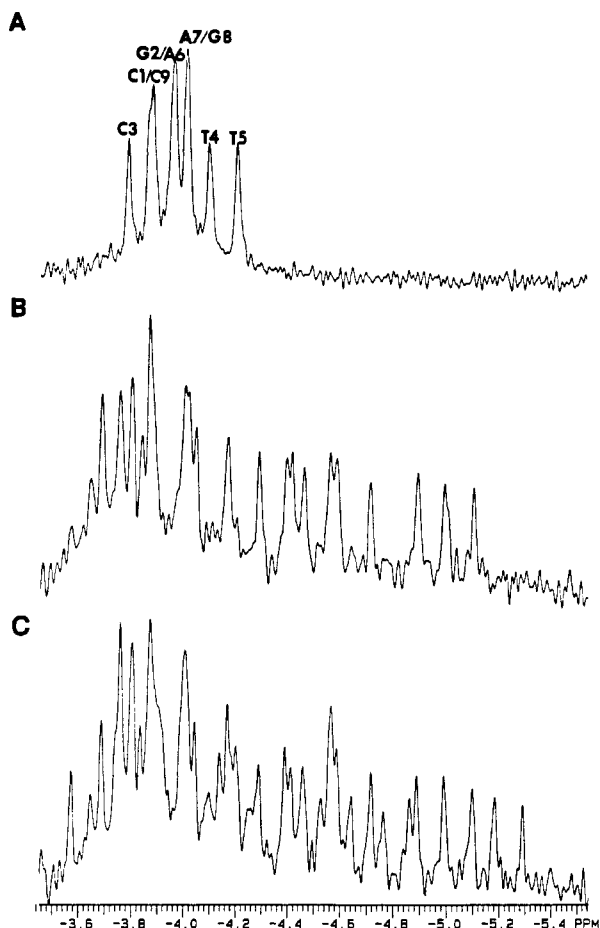


FIGURE 4: ^{31}P NMR spectra and phosphate assignments of decamer (numbering corresponds to phosphate position from the 5' end of the duplex) (A) and decamer-CPI-CDPI₂ complex after equilibration in buffer for several days (B) and taken immediately after dissolution of the lyophilized sample (C).

of months, slow depurination (and strand scission) remains unlikely. As described below, the presence of a minor adduct is also supported by the ^{31}P NMR and imino proton spectra.

Effect of CPI-CDPI₂ on the ^{31}P Spectrum of the Decamer. The ^{31}P NMR spectrum of the decamer is that expected for a small oligonucleotide duplex (Figure 4A). It contains six resonances covering an expected chemical shift range of -3.8 to -4.4 ppm (Gorenstein, 1984, 1987; Gorenstein et al., 1990). The signals have previously been identified through analysis of a 2D PAC spectrum (Powers et al., 1990).

The ^{31}P NMR spectrum of the decamer-drug complex is highly unusual, with dramatic upfield shifts up to 1.0 ppm (Figure 4B). Well-resolved peaks covering the entire chemical shift range of -3.6 to -5.3 ppm are noted. As far as we are aware, this effect on the ^{31}P spectrum upon binding a drug to a duplex has not been seen before (Gorenstein & Goldfield, 1984; Gorenstein et al., 1990). Typically, intercalating drugs cause 1–2 ppm downfield shifts, which reflects a local unwinding of the DNA helix as the phosphorus conformation changes from a *gauche*, *gauche* conformation to a *gauche*, *trans* conformation (Gorenstein & Kar, 1975; Gorenstein & Goldfield, 1984; Patel et al., 1982; Wilson et al., 1986). Minor groove binding drugs generally produce a small upfield shift of the ^{31}P signals (Gorenstein & Goldfield, 1984; Patel et al., 1982). The large upfield shifts caused by CPI-CDPI₂ are likely attributed to a strong shielding effect as opposed to a change in the DNA conformation.

The CPI-CDPI₂ structure has a natural curvature that resembles the DNA helical twist (Boger, personal communica-

tion). This curvature apparently facilitates the binding of CPI-CDPI₂ (as well as CC-1065) within the minor groove of the decamer, with the convex edge facing the minor groove (Boger et al., 1990; Boger & Coleman, 1988; Swenson et al., 1982a). On the basis of this model, the DNA phosphates will be located within the shielding cones of the aromatic residues of the drug. On the basis of the magnitude of the upfield shifts of the ^{31}P resonances, the phosphate residues must be quite close to CPI-CDPI₂'s aromatic residues. Thus in the duplex structure the imino protons are shifted 0.35–0.45 ppm upfield by shielding of the neighboring base pair which is 3.4 Å away (Giessner-Pretre et al., 1981; Giessner-Pretre & Pullman, 1987).

Interestingly, the ^{31}P spectrum of the decamer-CPI-CDPI₂ sample taken shortly after resolubilization from a lyophilized powder was more complex than the final spectrum shown in Figure 4B. This intermediate spectrum (Figure 4C) contained ca. 31 resonances of various intensities. The degeneracy of the phosphates in the two strands is lost in the duplex-drug complex, the expected number, this suggests that the initially prepared sample is heterogeneous, possibly representing two DNA-drug conformations.

The ^{31}P spectrum of the complex was retaken a few days after the original spectrum was taken. The second spectrum (Figure 4B) shows only 18–20 resonances of approximately equal intensity. The chemical shift range has also narrowed to -3.6 through -5.2 ppm. No further changes were observed in this final spectrum during the course of the study.

These changes in the ^{31}P spectrum of the decamer-CPI-CDPI₂ complex imply an initial heterogeneity in the complex which eventually equilibrates to largely a single conformation of the major adduct in solution. It should be noted that there are no phosphate monoester resonances that would be required if the sample had undergone depurination and β -elimination followed by strand scission. In addition, all of the ^1H NMR and detailed molecular modeling are consistent with an unaltered alkylated drug-duplex complex (all proton NMR spectra were taken after the sample had equilibrated). While the second ^{31}P spectrum indicated that most of this heterogeneity was lost with time, there is still an underlying broadness centered around -3.9 ppm and there are probably still more signals than can be accounted for by the 18 phosphorus resonances. This is attributable to the minor adduct or alternatively to several slow exchange conformational isomers.

Effect of CPI-CDPI₂ on the ^1H NMR Spectrum of the Decamer. The ^1H chemical shifts of the decamer were significantly perturbed upon binding CPI-CDPI₂. Upfield chemical shifts on the order of 0.5 ppm are observed for those protons proximal to the aromatic rings of the drug. Histogram plots comparing the chemical shifts of the H1', H2'/H2'', and H8/H6 protons with and without CPI-CDPI₂ are displayed in Figure 5. As observed in the ^{31}P spectrum, many of the protons are within the shielding cone of the aromatic rings of CPI-CDPI₂. Since the maximal effect was less than that which was seen for the ^{31}P resonances, the proton resonances must be further away from the drug's chromophores than at least some of the phosphate resonances.

The drug-induced perturbation in the ^1H chemical shifts of the decamer supports a point of alkylation at A17. This is consistent with the relatively large upfield shift (0.5 ppm) of the A17 H8 resonance. The next largest (Figure 5A) upfield shift of the aromatic resonances was to the bases on either side of A17 and corresponds to shifts of 0.2 ppm. The remainder of the aromatic base protons were only mildly perturbed either upfield or downfield by <0.1 ppm. It is reasonable that the

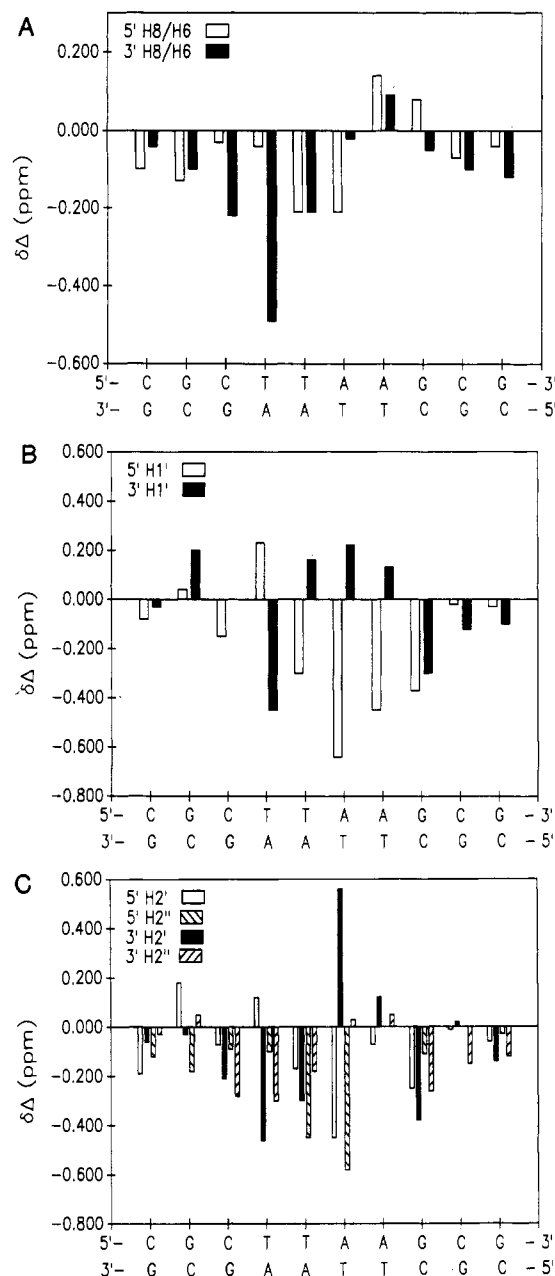


FIGURE 5: Histogram bar plot of differences in the ^1H chemical shifts $\Delta\delta$ between the decamer–CPI-CDPI₂ complex and duplex for the A strand (5') and alkylated B strand (3') (negative shift differences represent an upfield shift of the resonance in the drug complex). (A) A strand H8/H6 base protons (unfilled bar); B strand H8/H6 protons (filled bar). (B) A strand H1' protons (unfilled bar); B strand H1' protons (filled bar). (C) A strand H2' protons (unfilled bar); A strand H2'' protons (hatched bar); B strand H2' protons (filled bar); B strand H2'' protons (cross-hatched bar).

base which CPI-CDPI₂ alkylates will incur the greatest change in chemical shifts. This was further supported by the chemical shift perturbations of the H3' and H4' resonances of A17. These two resonances were also shifted dramatically upfield from the rest of the H3' and H4' protons. The H3' chemical shift decreased from 5.02 to 4.48 ppm, while the H4' chemical shift decreased from the 4.43 to 3.58 ppm. From model building of the CPI-CDPI₂ drug in the minor groove with alkylation occurring at N3 of A17, the H1' and H4' protons are the closest DNA protons to the drug, which could explain the large chemical shift effects. The H1' of A17 also was shifted 0.45 ppm upfield upon binding CPI-CDPI₂. The large upfield shift for all of the sugar and base H8 protons of A17 strongly supports this as the alkylation site of CPI-CDPI₂.

This binding mode was also generally supported by the pattern of shifts for the H1' protons in the drug adduct relative to those of the free decamer (Figure 5B). Interestingly, the largest upfield shift for an H1' proton is found for A6 on the nonalkylated A strand. Smaller downfield shifts on the H1' chemical shifts were observed at T14, T15, and A16. Indeed, the major perturbation of H1' chemical shifts on forming the adduct was upfield shifts from T4 through G8 on the A strand. Presumably this reflects a closer proximity of the aromatic rings to the A strand H1' protons. The downfield shifts for T14, T15, and T16 could be attributable to their location in the deshielding portion of the ring current cone. The H2' and H2'' (Figure 5C) show similar (although quite complicated) general upfield shifts in the adduct. All of these base and sugar proton chemical shift perturbations establish binding of the drug to the central AT-rich portion of the duplex. They are consistent with, although they do not prove, the suggestion that the drug binds to A17. The results also support the binding of the drug in the minor groove with the CDPI rings oriented toward the 5' end of the B strand.

Effect of CPI-CDPI₂ on the Decamer's Imino Resonances. The decamer's imino region contains three resonances at 12.55, 13.40, and 13.90 ppm (Figure 3 of the supplementary material). The assignment of the imino resonances can be tentatively determined by the relative chemical shifts and the melting profiles of the resonances. The decamer sequence contains ten imino protons, but by symmetry there should be a maximum of five unique imino resonances. The relative intensity of the three observed imino resonances corresponds to an approximate ratio of 1:2:2 relative to the most downfield resonance. The nature of the WS1D pulse sequence generates a sinusoidal pattern of signal intensity resulting in an inherent inaccuracy in measuring peak integrations (Sklenar & Bax, 1987). From the decamer sequence a tentative assignment was made of the imino resonances. The most downfield resonance was assigned to the first AT base pair from the end, whereas the most upfield resonance was assigned to the two internal GC base pairs. The central resonance was assigned to the terminal GC base pair and the internal AT base pair. This was supported by the observation that the two most downfield resonances demonstrated a lower melting temperature relative to the upfield resonance. The upfield resonance was assigned to the internal GC base pairs which should have the highest melting temperature.

Formation of the CPI-CDPI₂ adduct produced similar perturbations on the decamer's imino spectrum as was seen with the ^{31}P and nonexchangeable ^1H spectra (Figure 3B of the supplementary material). The decamer's imino spectrum also experienced a loss of degeneracy plus the generation of additional minor intensity resonances upon formation of the adduct. The relative chemical shifts of the imino protons were also perturbed. The two resonances at 11.2 and 11.7 ppm were tentatively assigned to the exchangeable protons of the drug. This assignment was based on the drug's spectra in DMSO where the labile NH resonances showed similar chemical shifts. In addition, if these resonances did correspond to DNA imino protons, it would imply a region of non-hydrogen-bonded bases since only non-hydrogen-bonded imino protons occur this far upfield. This seems unlikely since the presence of CPI-CDPI₂ stabilized the decamer helical structure.

The imino resonances of the free decamer are completely undetectable at 30 °C as the base pairing is disrupted, allowing for rapid exchange of the imino protons with water. In contrast, a significant amount of intensity is still observed at 30 °C for the decamer–CPI-CDPI₂ complex. This demonstrates

CPI-CDPI₂'s ability to stabilize the duplex. The imino spectrum was not measured above 35 °C to avoid strand scission of the adduct. By comparing the relative intensity and line width of the complex's imino resonance at 30–35 °C to that of the free decamer, it is likely that the melting temperature of the adduct is increased by approximately 15–20 °C, which is similar to the observed stabilization monitored by UV melting.

The imino spectrum of the decamer–CPI-CDPI₂ complex also supports a dynamic exchange between multiple conformations. These multiple conformations seem to have been "frozen" out at low temperature. The 5 °C spectrum of the complex contains two very weak peaks at 14.45 and 13.9 ppm. The major imino resonance at 13.6 ppm has a broad shoulder resonance, and there is significant intensity underlying the other major imino resonances. These additional resonances are relatively broader than the major imino resonances and disappear relatively quickly with an increase in temperature. Also, the additional resonances appear to converge with the major imino resonances with temperature. These characteristics of the decamer–CPI-CDPI₂ complex's imino spectrum is consistent with a transfer from slow exchange to a fast exchange on the NMR time scale with temperature.

Other evidence supporting a conformational equilibrium arises from a comparison of the decamer and the decamer–CPI-CDPI₂ imino resonances' line width. The decamer's imino resonances had an average line width of 30 Hz at 5 °C while the adduct's spectrum had an average line width of 45 Hz at 5 °C. The decamer spectrum exhibited typical characteristics as the temperature increases. The line width narrows initially as the temperature increases followed by a great increase in the line widths at higher temperatures, whereas the line widths of the complex decrease linearly to an average value of 11 Hz at 35 °C. The major factor affecting the line widths of imino protons is exchange with H₂O, which increases with temperature as the helix denatures—resulting in broad lines. The initially large line widths and subsequent narrowing of the complex's imino resonances must represent another exchange phenomena. This additional exchange phenomena is possibly an exchange between two adduct conformations.

Spin-Lattice Relaxation Times of the Decamer and the Complex. The spin-lattice relaxation times can reflect local structure since it is dependent on local correlation times and relaxation pathways. As found for the decamer, the adenosine H2 protons generally have long relaxation times (ca. 5 s), since they are a relatively isolated spin system. In contrast, the other aromatic resonances had typical T_1 times of 1.2–2.0 s.

The binding of CPI-CDPI₂ did have a significant effect on the adenosine H2 T_1 relaxation times. The T_1 values of all the aromatic resonances including the H2 signals were within the range of 1.1–1.7 s. This decrease in the adenosine H2 T_1 relaxation times indicates that additional relaxation pathways are introduced when the drug is bound to the decamer. This supports the proposed binding of the drug at A17 since it places the drug near all four adenosine bases. Indeed, in the refined structure of the adduct all of the adenosine H2 resonances are within 3 Å of CPI-CDPI₂ protons.

Restrained Molecular Dynamics Refinement of the Decamer–CPI-CDPI₂ Complex. As described under Experimental Procedures, NOESY distance restrained structural refinement of the model-built decamer–CPI-CDPI₂ complex utilized an iterative hybrid relaxation matrix methodology as implemented in the program MORASS (Meadows et al., 1989; Post et al., 1990). The NOESY distance restrained molecular dynamics refinement against the experimental NOESY vol-

umes proceeded in two stages. Initially, the decamer was refined alone with NOESY data corresponding to intra/inter DNA distances. Initial distances were calculated by integrating the cross-peaks and utilizing the two-spin approximation at short mixing times (Table III; Wuthrich, 1986). The two-spin methodology assumes that at very short mixing times in the linear regime of the NOE buildup the cross-peak intensity of a spin pair is inversely proportional to the sixth power of the distance between those two protons. The NOESY-derived distances were then used in a distance-constrained energy minimization (AMBER) of the decamer duplex structure. Instead of a simple harmonic potential error function to restrain the NMR-derived distances, we have modified AMBER so as to provide a flatwell harmonic function which we believe better reflects the intrinsic accuracy of these NOESY distance restraints (Clare et al., 1985; Schroeder et al., 1986; Gorenstein et al., 1990). The left and right force constants in the flatwell harmonic potential for the NOESY distance constraint term were set to 20 kcal/(mol·Å²) with permitted errors of $\pm 15\%$ in the NOESY distances. The total energy and constraint violation energy term is shown in the MIN entry in Table IV.

These "two-spin distances" were derived from a 250-ms mixing time NOESY spectrum, which was necessary in order to obtain additional and more accurately integrated NOESY cross-peaks for further refinement of the structures. Unfortunately, spin diffusion effects for such a long mixing time NOESY experiment introduce considerable errors in the calculated distances from the isolated two-spin approximation methodology (errors analyzed by using MORASS may be as large as 1.3 Å for distances of ca. 4.5 Å; Post et al., 1990; Gorenstein et al., 1990). The 150-ms mixing time NOESY was not used because many of the cross-peaks were too weak to quantify accurately. The 400-ms spectrum was qualitatively comparable to the 250-ms spectrum.

Therefore, the hybrid matrix procedure was employed to correct for multispin effects at this longer mixing time. The typical refinement follows the iterative merged matrix/restrained molecular dynamics methodology incorporating the NOESY distance constraints as described previously. A single isotropic correlation time model was employed to calculate the cross relaxation rates, σ_{ij} , and the direct longitudinal relaxation rates (Nikonowicz et al., 1990). We have based our correlation time on the Stokes–Einstein relationship as well as estimates from the ¹H T_1 relaxation times. We have shown (Meadows, unpublished results) that, with proper scaling of the experimental to the theoretically calculated volumes, an incorrect estimate of τ_c has negligible effects on the derived distances within limits (up to mixing times between 250 and 300 ms for values of τ_c from ca. 3.5 to 6.0 ns for the decamer). We are therefore confident that although our method is in part dependent on a reasonably correct τ_c estimate, much of the potential error possibly introduced by the choice of a poor τ_c is corrected by scaling at each merging cycle. A stepwise or perturbational merging was implemented to improve the diagonalization behavior of the hybrid volume matrix. After the intensity matrix is calculated and the data sets are scaled, the intensities of cross-peaks measurable by NOESY are compared (Nikonowicz et al., 1989; Gorenstein et al., 1990). The perturbational approach involves the substitution of only a fraction of the experimentally determined volumes. This "gentle nudging" of the intermediate structures avoids dramatic changes in one iteration which can produce an ill-conditioned mathematical problem during the transformation of the incorrect initial structure to the final structure. Full merging occurred by the eighth iteration.

Table IV: Calculated Energies for the Decamer during Restrained Molecular Dynamics Structural Refinement Starting from the B-DNA Model

structure ^a	I ^b	energy ^c	constraints ^c	RMS ^d	%RMS(EXP) ^e	%RMS(THE) ^e	R ^f	RMS(dis) ^g
B-DNA		-874	0					3.12
MIN		-808	41.1					3.09
MORASS	1	-689	121.8	4.59	282.0	70.2	0.70	2.11
MORASS	2	-752	70.5	3.16	140.8	59.5	0.47	1.95
MORASS	3	-821	23.0	2.90	114.2	49.4	0.40	2.39
MORASS	4	-518	190.5	2.83	101.2	50.5	0.38	2.71
MORASS	5	-632	122.2	3.14	67.6	52.0	0.34	2.56
MORASS	6	-606	128.7	2.45	107.0	45.1	0.37	2.65
MORASS	7	-671	96.9	3.04	88.6	54.2	0.34	2.26
MORASS	8	-670	104.2	2.35	103.4	43.4	0.32	
MORASS	9	-605	136.7	2.69	67.1	47.6	0.31	2.81
CPI MIN		-646	138.4					2.81
MORASS	10	-644	150.9	2.73	75.9	52.4	0.34	1.57
MORASS	11	-716	123.2	2.33	78.9	44.9	0.31	0.00
MORASS	12	-787	87.3	2.35	63.5	43.3	0.30	

^aStructure identifiers: B-DNA, Arnott model-built structure; MIN, minimization with two-spin constraints; MORASS, MORASS iteration; CPI, addition of CPI-CDPI₂ to the structure. ^bMORASS iteration number. Iterations 1–9 included only the DNA. Iterations 10–12 included the full DNA agent structure. ^cThe total energy (kcal/mol) of the structure from the AMBER minimization of the 3–5-ps dynamics-averaged structure and the corresponding constraint energy. Constraints for the two-spin minimization were 20 kcal/mol and a 15% allowed error. Constraints for MORASS iterations 1–3 were 20 kcal/mol with a 10% allowed error in the flatwell distance-constraining harmonic term. For iterations 4–12, a 30 kcal/mol and a 5% allowed error were used. ^dRMS difference (eq 1) between the experimental and theoretical volumes. ^e%RMS difference 9eq 1) between the experimental and theoretical volumes relative to either experimental volumes (EXP) or theoretical volumes (THE). ^fR factor (eq 2). ^gRMS difference in angstroms between the final structure and each structure during the refinement.

This basic iterative scheme was followed until the %RMS (eq 1) converged to a limiting value as outlined in Table IV. After the third 5-ps cycle, the distance-constraining pseudo force constants were increased and the estimated error brackets were decreased. Table IV lists energies, RMS percent volume differences, and the *R* factor (eq 2) at various iteration cycles.

After nine MORASS/MD cycles of 5 ps each the %RMS-(EXP) error between the experimental volumes and the theoretical volumes of the DNA portion of the drug duplex complex was reduced from 282% to 67% [similar reductions in the %RMS(THE) and the *R* factor are also observed]. Note that errors of 60–70% in the volumes represent an error of only ca. 12% in the distances because of the inverse sixth power dependence of the volumes on the distances. At this stage the CPI-CDPI₂ was docked onto the decamer with the alkylation at the N3 of A17, which is consistent with the drug–DNA NOESY cross-peaks of Figure 3 and the chemical shift perturbations. The adduct was then refined in cycles 10–12, although *no* drug–DNA NOESY cross-peaks were included in this second refinement stage. In this final model the calculated distances were qualitatively consistent (<6 Å ± 40%) with the intensities of the observed NOESY drug–DNA cross-peaks. This methodology eliminated difficulties that occurred when the intact decamer–CPI-CDPI₂ complex was used. The major difficulty that occurred when the refinement procedure used the decamer–CPI-CDPI₂ complex as the initial structure was the observed motion of CPI-CDPI₂ during the restrained molecular dynamics calculations. During the dynamics run, the second CDPI residue flipped from its initial edge-on conformation to a face-on conformation in the minor groove. This motion occurred within the first 2 ps of the restrained dynamics, and this residue remained in the face-on conformation. As the iteration procedure continued, the first CDPI residue also flipped from its initial edge-on conformation to a face-on conformation in the minor groove. This motion occurred within the first 10 ps of restrained dynamics. A 20-ps unrestrained dynamics calculation of the CPI-CDPI₂ molecule alone was done to determine if this motion of the drug in the complex was unique to the complex structure. During the entire 20-ps dynamics, the second CDPI residue made one 180° rotation about the amide linkage connecting the two CDPI residues. Thus isomerization about the amide linkages in the drug and drug–duplex complex is

feasible. This motion of the drug moiety in the complex distorted the structure of the decamer and in particular induced a large increase in the width of the minor groove. Further MORASS/dynamics calculations did not lead to any further refinement; indeed, the structure continued to distort further, and various %RMS and *R* factors increased at each iteration cycle. However, when CPI-CDPI₂ was docked onto the decamer after the MORASS refinement of the DNA portion of the drug complex was complete, the exaggerated distortion of the drug and duplex structures did not occur and further refinement of the complex was possible.

While the total minimized energies and the constraint energy term shown in Table IV appear to increase as the refinement progresses, this is attributed to the variation in the constraining distances during the MORASS hybrid matrix calculation, the increasing constraint force constants, and the narrower error limits imposed on the structures in later iterations.

A comparison of the initial model-built and final refined CPI-CDPI₂–decamer complex structure is shown in Figure 6. An RMS comparison of the changes in the Cartesian coordinates of the structures at various refinement stages is also listed in Table IV.

The initial model of the CPI-CDPI₂ docked into the minor groove of a model-built duplex decamer has the CPI-CDPI₂ edge on in the minor groove at an approximate 45° angle relative to the DNA axis, and the width of the minor groove (6.5 Å) is consistent with a B-DNA model. The final refined complex structure is quite different. The drug is now orientated approximately parallel with the DNA axis, and the minor groove has opened up to an average width of 9.5 Å. The most striking change in the DNA's structure is the kink that occurs abruptly at the CPI-CDPI₂ alkylation site. This kink bends the DNA at an approximate 60° angle from the DNA axis. The presence of this kink in the DNA's axis allows the CPI and the second CDPI residue to lie in the minor groove slightly rotated from an edge-on orientation to a partial face-on orientation. This occurs without any distortion or rotation of the CPI-CDPI₂ structure. Thus, on the basis of the results of the refinement of the complex, CPI-CDPI₂ prefers to be rotated from a complete edge-on conformation and it obtains this orientation by significantly distorting the DNA structure. Note that the distorted DNA structure was obtained strictly from refinement with experimental DNA NOEs, and no major

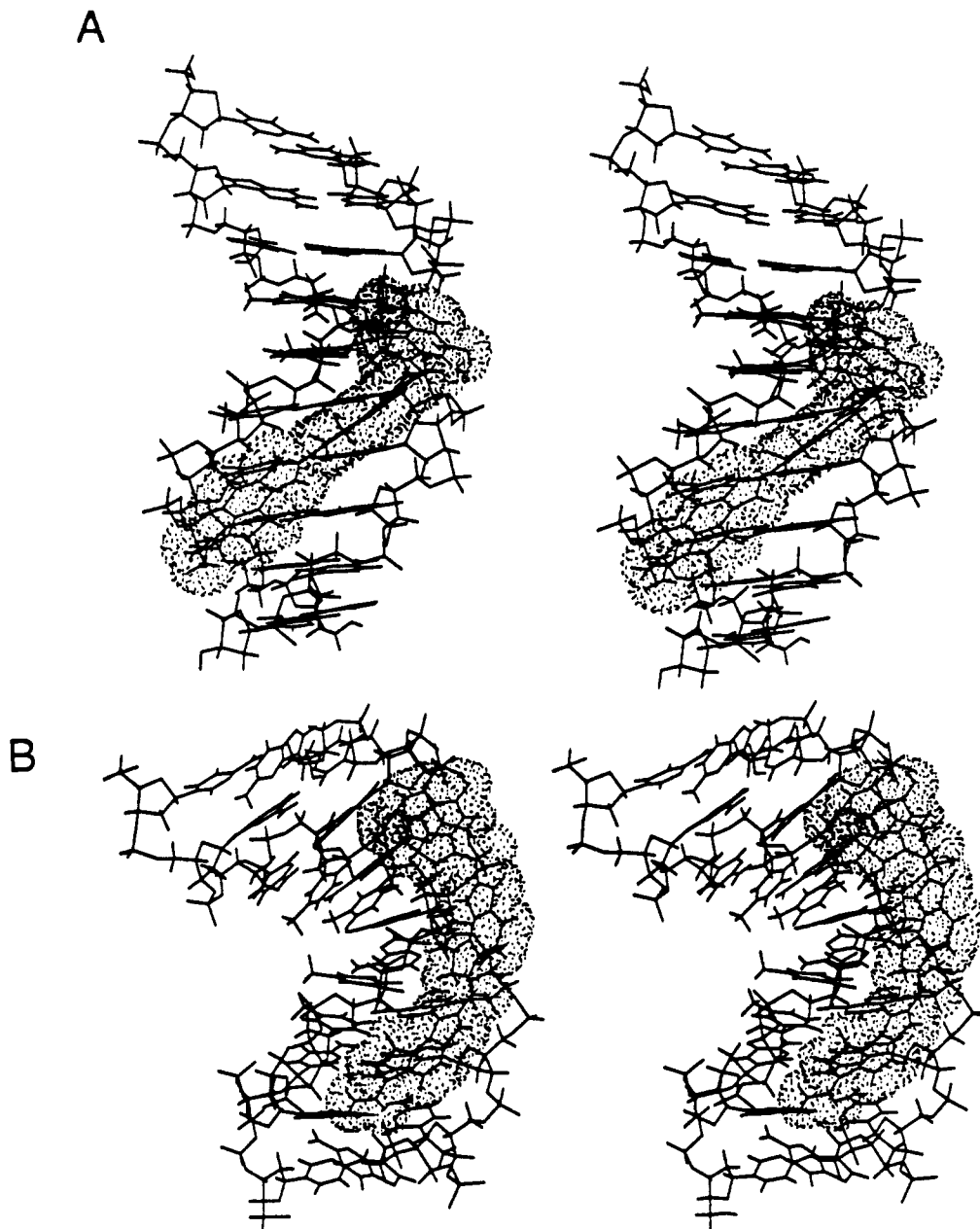


FIGURE 6: Stereoviews of (A) the initial model involving docking of the CPI-CDPI₂ (dotted van der Waals surface is shown) to a regular B-DNA decamer and (B) NOESY distance restrained, MORASS hybrid matrix/molecular dynamics final refined structure of the decamer-CPI-CDPI₂ complex starting from the initial model. The A strand C1 is depicted in the upper left of the structures with the minor groove at A17 facing away or to the right of the viewer. Note the sharp bend in the duplex near the site of alkylation in B.

change in the structure occurred after the CPI-CDPI₂ molecule was redocked onto the decamer. Even though refinement was based only upon the DNA-DNA distances, the derived two-spin distances from the NOESY spectra between drug-drug and drug-DNA protons are generally consistent with the final refined model. On the basis of the final %RMS of 67%, the DNA-DNA distances are reliable to an overall average of $\pm 12\%$. However, because the ¹H NMR assignments of the drug need further confirmation and no refinement was made on the basis of the drug-DNA distances, the refined model for the decamer-CPI-CDPI₂ complex must be regarded as speculative at this stage. The structure is, however, internally consistent with the NOESY and chemical shift perturbation results.

Conclusion. Structural information on a d-(CGCTTAAGCG)₂-CPI-CDPI₂ complex has been provided by NMR spectroscopy. The presence of the drug removed the degeneracy in the palindromic decamer's ¹H NMR, ³¹P NMR,

and the imino proton spectra. CPI-CDPI₂ also induced upfield shifts of the ³¹P resonances and the H1' and H2'/H2'' protons. The induced upfield shifts were consistent with a minor groove model where the sugar ring protons and phosphorus atoms are within the shielding cones of the CPI-CDPI₂ chromophores. The effect of CPI-CDPI₂ on the ¹H chemical shifts of the decamer also indicated a possible point of alkylation. The presence of CPI-CDPI₂ caused a dramatic upfield shift of the A17 H8 resonances and a pattern of upfield shifts for the H1' protons consistent with positioning the CPI ring system at A17 and orienting the CDPI rings toward the 5' end of the alkylated (B) strand in the minor groove. The hybrid matrix (MORASS)/restrained molecular dynamics refinement of the model-built complex indicates a novel DNA structure induced by the presence of the CPI-CDPI₂. The presence of CPI-CDPI₂ causes a 60° kink in the DNA axis at the A17 alkylation site and widens the minor groove from 6.5 to 9.5 Å. The distortion of the decamer accommodates the preferred orien-

tation of CPI-CDPI₂ in the minor groove. It allows the drug to move from an entirely edge-on conformation to a partial face-on conformation.

There is currently much interest in sequence-specific bends in DNA structures [see DiGrabriele et al. (1989)]. These kinks appear to occur in AT-rich regions, similar to that found in the decamer CPI-CDPI₂ complex. Perhaps one factor in the selectivity of this agent for AT-rich regions is the favorable binding to these bent DNA structures.

The ¹H NMR spectrum of the complex supports a single major conformation of the decamer adduct which accounts for >90% of the observed NOEs. The assignment of the decamer's ¹H NMR spectrum in the complex indicates only one major sequential assignment pattern for the decamer. This supports the formation of one major adduct between CPI-CDPI₂ and the decamer. A possible explanation for the remaining unassigned resonances could be a second conformation of the decamer complex or the presence of a minor alkylation site (or orientation) complex.

ACKNOWLEDGMENTS

We express our appreciation to Drs. Dale Boger and Steven Munk for providing the CPI-CDPI₂ and for helping in the preparation of the adduct. We also appreciate the contributions of Drs. Claude Jones and Julian Tirado-Rives.

SUPPLEMENTARY MATERIAL AVAILABLE

Three figures showing the 1D and 2D ¹H NOESY spectra of the decamer and decamer-CPI-CDPI₂ complex as well as the 1D imino spectra (4 pages). Ordering information is given on any current masthead page.

REFERENCES

- Adams, E. G., Sadiner, G. J., & Bhuyan, B. K. (1988) *Cancer Res.* **48**, 109–116.
- Bax, A., & Freeman, R. (1982) *J. Am. Chem. Soc.* **104**, 1099–1100.
- Boelens, R., Koning, T. M. G., & Kaptein, R. (1988) *J. Mol. Struct.* **173**, 299–311.
- Boelens, R., Koning, T. M. G., van der Marel, G. A., van Boom, J. H., & Kaptein, R. (1989) *J. Magn. Reson.* **82**, 290–308.
- Boger, D. L., & Coleman, R. S. (1988) *J. Am. Chem. Soc.* **110**, 4796–4807.
- Boger, D. L., Coleman, R. S., Invergo, B. J., Sakya, S. M., Ishizaki, T., Munk, S. A., Zarrinmayeh, H., Kitos, P. A., & Thompson, S. C. (1990) *J. Am. Chem. Soc.* **112**, 4623–4632.
- Broido, M. A., Zon, G., & James, T. L. (1984) *Biochem. Biophys. Res. Commun.* **119**, 663–670.
- Canet, D., Levy, G. C., & Peat, J. R. (1975) *J. Magn. Reson.* **18**, 199–204.
- Chidester, C. G., Krueger, W. C., Mizsak, S. A., Duchamp, D. J., & Martin, D. G. (1981) *J. Am. Chem. Soc.* **103**, 7629–7635.
- Clare, G. M., Gronenborn, A. M., Brunger, A. T., & Karplus, M. (1985) *J. Mol. Biol.* **186**, 435–455.
- DiGrabriele, A. D., Sanderson, M. R., & Steitz, T. A. (1989) *Proc. Natl. Acad. Sci. U.S.A.* **86**, 1816–1820.
- Feigon, J., Leupin, W., Denny, W. A., & Kearns, D. R. (1983) *Biochemistry* **22**, 5930–5942; 5943–5951.
- Ferrin, T. E., & Langridge (1980) *Computer Graphics* **13**, 320.
- Frechet, D., Cheng, D. M., Kan, L.-S., & Ts'o, P. O. P. (1983) *Biochemistry* **22**, 5194–5200.
- Gait, M. J. (1984) *Oligonucleotide Synthesis: a Practical Approach*, IRL Press, Oxford.
- Giessner-Prettre, C., & Pullman, B. (1970) *J. Theor. Biol.* **27**, 87–95.
- Giessner-Prettre, C., & Pullman, B. (1987) *Q. Rev. Biophys.* **20**, 114–173.
- Gorenstein, D. G. (1984) *Phosphorus-31 NMR: Principles and Applications* (Gorenstein, D. G., Ed.) Academic Press, New York.
- Gorenstein, D. G. (1987) *Chem. Rev.* **87**, 1047–1077.
- Gorenstein, D. G., & Kar, D. (1975) *Biochem. Biophys. Res. Commun.* **65**, 1073.
- Gorenstein, D. G., & Goldfield, E. M. (1984) *³¹P NMR: Principles and Applications* (Gorenstein, D. G., Ed.) Academic Press, New York.
- Gorenstein, D. G., Meadows, R. P., Metz, J. T., Nikonowicz, E., & Post, C. P. (1990) *Advances in Biophysical Chemistry* C. A., (Bush, Ed.) JAI Press, Greenwich.
- Hanka, L. J., Dietz, A., Gerpheide, S. A., Kuentzel, S. L., & Martin, D. G. (1978) *J. Antibiot.* **31**, 1211.
- Hare, D. R., Wemmer, D. E., Chou, S. H., Drobny, G., & Reid, B. (1983) *J. Mol. Biol.* **171**, 319.
- Hurley, L. H., & Needham-VanDevanter, D. R. (1986) *Acc. Chem. Res.* **19**, 230–237.
- Hurley, L. H., Needham-VanDevanter, D. R., & Lee, C.-S. (1987) *Proc. Natl. Acad. Sci. U.S.A.* **84**, 6412–6416.
- Hurley, L. H., Warpehoski, M. A., Lee, C.-S., McGovern, J. P., Scahill, T. A., Kelly, R. C., Mitchell, M. A., Wicniewski, N. A., Gebhard, I., Johnson, P. D., & Bradford, V. S. (1990) *J. Am. Chem. Soc.* **112**, 4633–4649.
- Kearns, D. R. (1984) *Crit. Rev. Biochem.* **15**, 237–290.
- Krueger, W. C., & Prairie, M. D. (1987) *Chem.-Biol. Interact.* **62**, 281–295.
- Krueger, W. C., Li, L. H., Moscovitz, A., Prairie, M. D., Petzold, G., & Swenson, D. H. (1985) *Biopolymers* **24**, 1549–1572.
- Krueger, W. C., Duchamp, D. J., Li, L. H., Moscovitz, A., Petzold, G. L., Prairie, M. D., & Swenson, D. H. (1986) *Chem.-Biol. Interact.* **59**, 55–72.
- Martin, D. G., Chidester, C. G., Duchamp, D. J., & Mizsak, S. A. (1980) *J. Antibiot.* **33**, 902–903.
- Meadows, R., Post, C., & Gorenstein, D. G. (1989) MORASS Program, Purdue University, West Lafayette, IN.
- Moy, B. C., Prairie, M. D., Krueger, W. C., & Bhuyan, B. K. (1989) *Cancer Res.* **49**, 1983–1988.
- Needham-VanDevanter, D. R., Hurley, L. H., Reynolds, V. L., Theriault, N. Y., Krueger, W. C., & Wierenga, W. (1984) *Nucleic Acids Res.* **12**, 6159–6168.
- Nikonowicz, E., Meadows, R., Post, C., Jones, C., & Gorenstein, D. G. (1989) *Bull. Magn. Reson.* **11**, 226–229.
- Patel, D. J., Pardi, A., & Itakura, K. (1982) *Science* **216**, 581.
- Piantini, U., Sorensen, O. W., & Ernst, R. R. (1982) *J. Am. Chem. Soc.* **104**, 6800–6801.
- Post, C. B., Meadows, R., & Gorenstein, D. G. (1990) *J. Am. Chem. Soc.* (in press).
- Powers, R., Olsen, R. K., & Gorenstein, D. G. (1989) *J. Biomol. Struct. Dyn.* **7**, 515–556.
- Powers, R., Jones, C. R., & Gorenstein, D. G. (1990) *J. Biomol. Struct. Dyn.* (in press).
- Reynolds, V. L., Molineux, I. J., Kaplan, D. J., Swenson, D. H., & Hurley, L. H. (1985) *Biochemistry* **24**, 6228–6237.
- Reynolds, V. L., McGovern, J. P., & Hurley, L. H. (1986) *J. Antibiot.* **39**, 319–334.
- Scahill, T. A., Jensen, R. M., Swenson, D. H., Hatzenbuehler, N. T., Petzold, G., Wierenga, W., & Brahme, N. D. (1990) *Biochemistry* **29**, 2852–2860.

- Scheek, R. M., Boelens, R., Russo, N., Van Boom, J. H., & Kaptein, R. (1984) *Biochemistry* 23, 1371-1376.
- Schroeder, S., Jones, C., Fu, J., & Gorenstein, D. G. (1986) *Bull. Magn. Reson.* 8, 137-146.
- Schroeder, S. A., Fu, J. M., Jones, C. R., & Gorenstein, D. G. (1987) *Biochemistry* 26, 3812-3821.
- Sklenar, V., & Bax, A. (1987) *J. Magn. Reson.* 74, 469-479.
- States, D. J., Haberkorn, R. A., & Rueben, D. J. (1982) *J. Magn. Reson.* 48, 286-292.
- Swenson, D. H., Li, L. H., Hurley, L. H., Rokem, J. S., Petzold, G. L., Dayton, B. D., Wallace, T. L., & Lin, A. H. (1982a) *Cancer Res.* 42, 2821-2828.
- Swenson, D. H., Li, L. H., Hurley, L. H., Rokem, J. S., Petzold, G. L., Dayton, B. D., Wallace, T. L., & Lin, A. H. (1982b) *Cancer Res.* 42, 2821-2828.
- Warpehoski, M. A., Gebhard, I., Kelly, R. C., Krueger, W. C., Li, L. H., McGovern, J. P., Prairie, M. D., & Wicniewski, N. (1988) *J. Med. Chem.* 31, 590-603.
- Weiner, P. K., & Kollman, P. A. (1981) *J. Comput. Chem.* 2, 287-303.
- Wierenga, W., Bhuyan, B. K., Kelly, R. C., Krueger, W. C., Li, L. H., McGovern, J. P., Swenson, D. H., & Warpehoski, M. A. (1986) *Adv. Enzyme Regul.* 25, 141-155.
- Wilson, W. D., Jones, R. L., Zon, G., Scott, E. V., Banville, D. L., & Marzilli, L. G. (1986) *J. Am. Chem. Soc.* 108, 7113-7114.
- Wuthrich, K. (1986) *NMR of Proteins and Nucleic Acids*, Wiley, New York, NY.